Inorg. Chem. **2007**, *46*, 5196–5206

Coordination Mode of Nitrate in Uranyl(VI) Complexes: A First-Principles Molecular Dynamics Study

Michael Bühl,*,† Romain Diss,‡ and Georges Wipff‡

Max-Planck-Institut für Kohlenforschung, Kaiser-Wilhelm-Platz 1, D-45470 Mülheim an der Ruhr, Germany, and UMR 7177 CNRS, Laboratoire MSM, Institut de Chimie, 4 rue Blaise Pascal, 67000 Strasbourg, France

Received November 27, 2006

According to Car–Parrinello molecular dynamics simulations for $[UO_2(NO_3)_3]^-$, $[UO_2(NO_3)_4]^{2-}$, and $[UO_2(OH_2)_4(NO_3)]^+$ complexes in the gas phase and in aqueous solution, the nitrate coordination mode to uranyl depends on the interplay between ligand–metal attractions, interligand repulsions, and solvation. In the trinitrate, the η^2-coordination is clearly favored in water and in the gas phase, leading to a coordination number (CN) of 6. According to pointwise thermodynamic integration involving constrained molecular dynamics simulations, a change in free energy of +6 kcal/mol is predicted for η^2- to η^1-transition of one of the three nitrate ligands in the gas phase. In the gas phase, the mononitrate–hydrate complex also prefers a η^2-binding mode but with a CN of 5, one H_2O molecule being in the second shell. This contrasts with the aqueous solution where the nitrate binds in a η^1-fashion and uranyl coordinates to four H_2O ligands. A driving force of ca. –3 kcal/mol is predicted for the η^2- to η^1- transition in water. This structural preference is interpreted in terms of steric arguments and differential solvation of terminal vs uranyl-coordinated O atoms of the nitrate ligands. The $[UO_2(NO_3)_4]^{2-}$ complex with two η^2- and two η^1- coordinated nitrates, observed in the solid state, is stable for 1–2 ps in the gas phase and in solution. In the studied series, the modulation of uranyl–ligand distances upon immersion of the complex in water is found to depend on the nature of the ligand and the composition of the complex.

Introduction

The chelate effect is an important paradigm in coordination chemistry.[1] The enhanced stability of metal complexes with multidentate ligands, as compared to monodentate variants of these, is the key to a wide variety of applications in extraction processes, including separation of metals on a large scale or in vivo sequestration of potentially poisonous metals.[2] The common rationalization of this effect is based on the gain in entropy upon release of a certain number of monodentate ligands, such as solvent molecules from the first solvation sphere, upon chelate formation.[3] There is also evidence from quantum-chemical computations that, in some cases, for instance for lanthanide or actinide complexes with diamides, a large fraction of the driving force for chelate formation is enthalpic in nature.[4,5] According to quantum-chemical calculations at Hartree−Fock and DFT levels, typical chelating ligands such as malonamides and succinamides bind less strongly in bidentate fashion to uranyl than two corresponding monodentate analogs, with enthalpic differences up to 24 kcal/mol (B3LYP) in favor of the latter.[4b] In general, particularly stable complexes are formed when the resulting metallacyclic motifs involve five- or six-membered rings in an octahedral (or square planar) environment about the metal center, because this arrangement allows

* To whom correspondence should be addressed. E-mail: buehl@mpi-muelheim.mpg.de.
† Max-Planck-Institut für Kohlenforschung.
‡ Laboratoire MSM.

(1) See for instance: (a) Sawicki, M.; Siaugue, J.-M.; Jacopin, C.; Moulin, C.; Bailly, T.; Burgada, R.; Meunier, S.; Baret, P.; Pierre, J.-L.; Taran, S. *Chem.—Eur. J.* **2005**, *11*, 3689−3697. (b) Jain, V. K.; Pillai, S. G.; Pandya, R. A.; Agrawal, Y. K.; Shrivastav, P. S. *Talanta* **2005**, *65*, 466−475 and references cited therein.
(2) Gorden, A. E. V.; Xu, J. D.; Raymond, K. N.; Durbin, P. *Chem. Rev.* **2003**, *103*, 4207−4282.
(3) Vallet, V.; Wahlgren, U.; Grenthe, I. *J. Am. Chem. Soc.* **2003**, *125*, 14941−14950. Choppin, G. *J. Alloys Compd.* **1997**, *249*, 1−18. Hancock, R. D. *J. Chem. Educ.* **1992**, *69*, 615−621. Mathur, J. N.; Murali, M. S.; Nash, K. L. *Solvent Extr. Ion Exch.* **2002**, *19*, 357−390.
(4) (a) Coupez, B.; Boehme, C.; Wipff, G. *Phys. Chem. Chem. Phys.* **2002**, *4*, 5716−5729. (b) Coupez, B.; Wipff, G. *Inorg. Chem.* **2003**, *42*, 3693−3703.
(5) (a) Boehme, C.; Wipff, G. *Inorg. Chem.* **2002**, *42*, 727−737. (b) Boehme, C.; Coupez, B.; Wipff, G. *J. Phys. Chem. A* **2002**, *106*, 6487−6498.

10.1021/ic0622555 CCC: $37.00
Published on Web 05/25/2007

Scheme 1

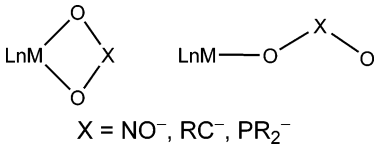

both for an ideal bite angle (90° in this case) and little or no strain in the chelate ring. The preference for multidentate bonding becomes less pronounced for four-membered rings and larger metal ions with less rigorous stereochemical requirements, as is the case for lanthanides or actinides. The most important ligands in this context are nitrate, carboxylates, and phosphates,[6] which can coordinate in η^2- or η^1-fashion (bi- or monodentate, respectively) as sketched in Scheme 1.

In an aqueous environment, the particular coordination mode adopted in such complexes can have a subtle but important effect on their solvation and, ultimately, extraction properties. The metal-bonded O atoms in the η^2-form tend to be less hydrophilic than the pendant anionic oxygen in the η^1-variant; i.e., the latter could be better solvated than the former. In this paper, we focus on uranyl−nitrate complexes as models for the species that are likely to be present in extraction of uranium in the PUREX process, after dissolution of spent nuclear fuel in 3−6 M nitric acid.[7,8]

Even though complexation constants between uranyl and nitrate ions are quite small in water,[9] there is spectroscopic evidence for formation of mono-, di-, and trinitrate species in aqueous solution,[9c,10] typically at elevated to very high nitrate concentrations. Mono- and trinitrate aquo complexes have also been reported in organic solutions of uranyl nitrate hydrate in the presence of alkyl phosphates that are commonly used for uranyl extraction.[11] Little is known from these solution studies concerning the nitrate binding mode, coordination number (CN) about uranyl, and precise U−O bond distances. Reliable structural information is available from single-crystal X-ray or neutron diffraction, albeit with unknown packing effects from the crystal matrix. Among the multitude of solid uranyl−nitrate complexes characterized so far,[12] binary species or those that contain only water as additional ligand comprise $UO_2(NO_3)_2(H_2O)_2$,[13] $[UO_2(NO_3)_3]^-$,[14] and $[UO_2(NO_3)_4]^{2-}$.[15] In the following, these complexes will be labeled **2**−**4**, respectively, according to the number of nitrate moieties. The tetranitrate **4** is of interest because it contains the nitrate ligand both in its usual η^2- as well as in the less common η^1-binding mode.[16,17]

Quantum-chemical computations can afford valuable insights into structure and energetics of uranyl complexes.[18] While medium effects are usually modeled implicitly by embedding the solute in a polarizable continuum, molecular dynamics (MD) simulations with explicit solvent (water) molecules can now be used to mimic the actual experimental conditions by including both specific and long-range solvent−solute interactions at ambient temperature.[19−21] We have been studying the well-known uranyl hydrate $[UO_2(H_2O)_5]^{2+}$ in aqueous solution using density-functional theory (DFT)-based Car−Parrinello MD (CPMD) simulations.[20] These studies corroborated the preference of five-coordination for

(6) For salient reviews, see e.g.: (a) Casellato, U.; Vigato, P. A.; Vidali, M. *Coord. Chem. Rev.* **1981**, *36*, 183−265. (b) Clark, D. L.; Hobart, D. E.; Neu, M. P. *Chem. Rev.* **1995**, *95*, 25−48. (c) Clearfield, A. *Curr. Opin. Solid State Mater. Sci.* **2002**, *6*, 495−506.

(7) McKibben, J. M. *Radiochim. Acta* **1984**, *36*, 3−15.

(8) Paiva, A. P.; Malik, P. *J. Radioanal. Nucl. Chem.* **2004**, *261*, 485−496.

(9) Extrapolated to standard conditions, a value of $\log_{10} \beta_1{}^0 = 0.30 \pm 0.15$ has been recommended for the equilibrium constant in the aqueous system $UO_2{}^{2+} + NO_3{}^- \rightleftharpoons UO_2NO_3{}^+$; see: (a) Grenthe, I.; Fuger, J.; Konings, R. J. M.; Lemire, R. J.; Muller, A. B.; Nguyen-trung, C.; Wanner, H. *Chemical Thermodynamics Vol. 1: Chemical Thermodynamics of Uranium*; Wanner, H.; Forest, I., Eds.; Elsevier: Amsterdam, 1992. Formation constants for uranyl dinitrate complexes are indicated to be smaller than for the mononitrate by roughly 1 order of magnitude. For results from an extraction-based method, see: (b) Lahr, H.; Knoch, W. *Radiochim. Acta* **1970**, *13*, 1−5. For results from a ^{1}H NMR spectroscopic study in water−acetone mixtures, see: (c) Fratiello, A.; Kubo, V.; Lee, R. E.; Schuster, R. E. *J. Phys. Chem.* **1970**, *74*, 3726−3730.

(10) De Houwer, S.; Görller-Walrand. *J. Alloys Compd.* **2001**, *323*−*324*, 683−687.

(11) Fedorov, Y. S.; Zilberman, B. Y. *Radiochemistry* **2000**, *42*, 242−246.

(12) A search in the Cambridge Structure database (version 5.27, Aug 2006) returns nearly 150 entries with a $U(NO_3)$ fragment.

(13) A search for the $UO_2(NO_3)_2(OH_2)_2$ fragment in the Cambridge Structure Database affords 15 hits containing **2**. For an early neutron-diffraction study, see: (a) Dalley, N. K.; Mueller, M. H.; Simonsen, S. H. *Inorg. Chem.* **1971**, *10*, 323−328. For a recent determination by X-ray crystallography, see e.g.: (b) Villiers, C.; Thuery, P.; Ephritikhine, M. *Polyhedron* **2004**, *23*, 1613−1618.

(14) See for instance: Crawford, M.-J.; Mayer, P. *Inorg. Chem.* **2005**, *44*, 8481−8485 and references cited therein.

(15) For a recent example (with dialkylimidazolium counterions, CSD refcodes IXULAO and IXUMAP), see e.g.: Bradley, A. E.; Hardacre, C.; Nieuwenhuyzen, M.; Pitner, W. R.; Sanders, D.; Seddon, K. R.; Thied, R. C. *Inorg. Chem.* **2004**, *43*, 2503−2514.

(16) In solid-state structures the bidentate binding mode is found for the overwhelming majority of uranyl−nitrate complexes characterized so far; see e.g.: Burns, J. H. Structural Chemistry. In *The Chemistry of the Actinide Elements*, 2nd ed.; Katz, J. J., Seaborg, G. T., Morss, L. R., Eds.; Chapman and Hall: New York, 1986; Vol. 2, Chapter 20, pp 1417−1479.

(17) A few other cases of η^1-bonded nitrate complexes are known in uranyl dinitrates containing additional chelating ligands, for instance the following. (a) With the 1,3-diphenylpropane-1,3-dionato ligand (CSD ref-code PPNXUA): Graziani, R.; Marangoni, G.; Paolucci, P.; Forsellini, E. *J. Chem. Soc., Dalton Trans.* **1987**, 818−826. (b) With *p*-methyl-*N*-benzyltetrahomodiazacalix[4]arene (CSD refcode QETDEY): Thuéry, P.; Nierlich, M.; Vicens, J.; Masci, B.; Takemura, H. *Eur. J. Inorg. Chem.* **2001**, 637−643. (c) With terpyridine (CSD refcode AZECOX): Charushnikova, I. A.; Den, A. C. *Russ. J. Coord. Chem.* **2004**, *30*, 511−519. (d) With *N*-(2′-(dimethylamino)ethyl)-2-(aminoethyl)salicylaldiminato anion (refcode EASULU): Bandoli, G.; Clemente, D. A.; Cingi, M. B. *J. Inorg. Nucl. Chem.* **1975**, *37*, 1709−1714. (e) With 2,6-diacetylpyridinebis(2′-pyridinylhydrazone) (refcode NDAPUO10): Paolucci, G.; Marangoni, G.; Bandoli, G.; Clemente, D. A. *J. Chem. Soc., Dalton Trans.* **1980**, 459−466.

(18) Review: Vallet, V.; Macak, P.; Wahlgren, U.; Grenthe, I. *Theor. Chem. Acc.* **2006**, *115*, 145−160.

(19) For hybrid quantum-mechanical/molecular-mechanical MD, see: Infante, I.; Visscher, L. *J. Comput. Chem.* **2003**, *25*, 386−392.

(20) For Car−Parrinello MD, see: (a) Bühl, M.; Diss, R.; Wipff, G. *J. Am. Chem. Soc.* **2005**, *127*, 13506−13507. (b) Bühl, M.; Kabrede, H.; Diss, R.; Wipff, G. *J. Am. Chem. Soc.* **2006**, *128*, 6357−6368. (c) Bühl, M.; Kabrede, H. *Inorg. Chem.* **2006**, *45*, 3834−3836. (d) Bühl, M.; Kabrede, H. *ChemPhysChem* **2006**, *7*, 2290−2293.

(21) For classical molecular-mechanical MD, see e.g.: (a) Guilbaud, P.; Wipff, G. *J. Mol. Struct.* **1996**, *366*, 55−63. For more recent examples, see: (b) Baaden, M.; Schurhammer, R.; Wipff, G. *J. Phys. Chem. B* **2002**, *106*, 434−441. (c) Chaumont, A.; Engler, E.; Wipff, G. *Inorg. Chem.* **2003**, *42*, 5348−5356. (d) Chaumont, A.; Wipff, G. *Chem.−Eur. J.* **2004**, *10*, 3919−3930. (e) Galand, N.; Wipff, G. *J. Phys. Chem. B* **2005**, *109*, 277−287.

this complex in water[20a,c] and were able to qualitatively reproduce experimental energetic data, namely the barrier for water exchange[20c] and the acidity constant[20d] of uranyl hydrate.

For uranyl dinitrate **2**, the CPMD simulations showed that when going from the gas phase to an aqueous solution, the U−O(nitrate)and U−O(water) bonds become longer and shorter, respectively.[20b] In both environments, the nitrate ligands prefer to be η^2 -coordinated, but solvation facilitates the η^2-to-η^1 transition of one nitrate ligand in **2** noticeably. In water, the η^1-complex was indicated to be less stable than the η^2 form by only 1.4 kcal/mol.[20b] Apparently, the equilibrium between the coordination modes in Scheme 1 can be finely balanced for uranyl nitrate complexes. We now extend these studies to other uranyl complexes with different numbers of nitrate ligands, specifically to the trinitrate **3** and to the mononitrate complex $[UO_2(NO_3)(H_2O)_4]^+$ (**1**), where the two nitrate binding modes are considered. Together with **2**, these ions are expected to become important in the uranyl speciation at high concentration of nitric acid. Even though not immediately relevant for the solution chemistry, the gas phase and solution structures of the tetranitrate **4** are also considered for completion. Our simulations on **1**, **3**, and **4** do not aim at assessing the stabilities of these complexes in water but mainly at analyzing the effect of the polar environment on their precise structure as a function of the nitrate binding mode and the hydration number of uranyl.

Computational Details

The same methods and basis sets as in our previous study of **2**[20b] were employed. Specifically, geometries were optimized using the BLYP functional,[22] in conjunction with a variety of computational approaches: LANL denotes calculations performed with the Gaussian 03 program[23] employing the Los Alamos relativistic effective core potential for U together with its (3s3p2d2f) valence basis of contracted Gaussians, [24] standard 6-31G(d) basis for all other elements, and a medium-sized integration grid (75 radial shells with 302 angular points/shell).

ZORA[25,26] stands for scalar relativistic calculations using the approximation with the same name (zeroth-order relativistic approximation), a polarized triple-ζ basis of Slater functions for all elements, and a dense integration grid (ACCINT parameter equal to 6). The frozen-core approach was used.[27] Additional optimizations, labeled ZORA(aq), were performed in a polarizable continuum employing the COSMO variant,[28] the parameters of water, and a molecule-shaped cavity (defined as solvent-excluding surface with solvent radius of 1.4 Å and the following atomic radii in Å: U, 1.86; Cl, 1.75; O, 1.52; N, 1.55; C, 1.70; H, 1.20). All ZORA computations were performed with the ADF program package.[29]

CP-opt denotes geometries optimized using the density-functional-based Car−Parrinello scheme[30] as implemented in the CPMD program,[31] until the maximum gradient was less than 5×10^{-4} au. Norm-conserving pseudopotentials were used that had been generated according to the Troullier and Martins procedure[32] and transformed into the Kleinman−Bylander form.[33] For uranium, the semicore (or small-core) pseudopotential was employed that had been generated and validated in ref 20a. Periodic boundary conditions were imposed using cubic or orthorhombic supercells adjusted to the size of the complexes ($13 \times 13 \times 13$ Å^3 for **1** and $16 \times 13 \times 16$ Å^3 for **3** and **4**). Kohn−Sham orbitals were expanded in plane waves at the Γ-point up to a kinetic energy cutoff of 80 Ry. For the complexes in vacuo, Car−Parrinello molecular dynamics simulations (denoted CPMD) were performed in the NVT ensemble using a single Nosé-Hoover thermostat set to 300 K (instantaneous heat-up, frequency 1800 cm^{-1}), a fictitious electronic mass of 600 au, and a time step of 0.121 fs. These unconstrained simulations were followed over 2−4 ps, the first 0.5 ps of which was taken for equilibration.[34] For the aqueous solutions, labeled CPMD(aq), the boxes were filled with 54, 90, and 86 water molecules for **1**, **3**, and **4**, respectively, affording a density of 1.1, corresponding to that of typical uranyl complexes (e.g., uranyl nitrate) with similar concentration.[35] To increase the time step, hydrogen was substituted with deuterium. Long-range electrostatic

(22) (a) Becke, A. D. *Phys. Rev. A* **1988**, *38*, 3098−3100. (b) Lee, C.; Yang, W.; Parr, R. G. *Phys. Rev. B* **1988**, *37*, 785−789.

(23) Frisch, M. J.; Trucks, G. W.; Schlegel, H. B.; Scuseria, G. E.; Robb, M. A.; Cheeseman, J. R.; Montgomery, J. A., Jr.; Vreven, T.; Kudin, K. N.; Burant, J. C.; Millam, J. M.; Iyengar, S. S.; Tomasi, J.; Barone, V.; Mennucci, B.; Cossi, M.; Scalmani, G.; Rega, N.; Petersson, G. A.; Nakatsuji, H.; Hada, M.; Ehara, M.; Toyota, K.; Fukuda, R.; Hasegawa, J.; Ishida, M.; Nakajima, T.; Honda, Y.; Kitao, O.; Nakai, H.; Klene, M.; Li, X.; Knox, J. E.; Hratchian, H. P.; Cross, J. B.; Adamo, C.; Jaramillo, J.; Gomperts, R.; Stratmann, R. E.; Yazyev, O.; Austin, A. J.; Cammi, R.; Pomelli, C.; Ochterski, J. W.; Ayala, P. Y.; Morokuma, K.; Voth, G. A.; Salvador, P.; Dannenberg, J. J.; Zakrzewski, V. G.; Dapprich, S.; Daniels, A. D.; Strain, M. C.; Farkas, O.; Malick, D. K.; Rabuck, A. D.; Raghavachari, K.; Foresman, J. B.; Ortiz, J. V.; Cui, Q.; Baboul, A. G.; Clifford, S.; Cioslowski, J.; Stefanov, B. B.; Liu, G.; Liashenko, A.; Piskorz, P.; Komaromi, I.; Martin, R. L.; Fox, D. J.; Keith, T.; Al-Laham, Peng, M. A.; C. Y.; Nanayakkara, A.; Challacombe, M.; Gill, P. M. W.; Johnson, B.; Chen, W.; Wong, M. W.; Gonzalez, C.; Pople, J. A. *Gaussian 03*; Gaussian, Inc.: Pittsburgh, PA, 2003.

(24) Ortiz, J. V.; Hay, P. J.; Martin, R. L. *J. Am. Chem. Soc*. **1992**, *114*, 2736−2737 and references cited therein.

(25) (a) van Lenthe, E.; Baerends, E. J.; Snijders, J. G. *J. Chem. Phys*. **1993**, *99*, 4597−4610. (b) van Lenthe, E.; Baerends, E. J.; Snijders, J. G. *J. Chem. Phys.* **1994**, *101*, 9783−9792. (c) van Lenthe, E.; Ehlers, A. E.; Baerends, E. J. *J. Chem. Phys.* **1999**, *110*, 8943−8953.

(26) Wolff, S. K; Ziegler, T.; van Lenthe, E.; Baerends, E. J. *J. Chem. Phys.* **1999**, *110*, 7689−7698.

(27) The frozen core electrons are the 1s shell for C, O, and N, 1s, 2s, and 2p for Cl, and 1s, 2s, 2p, 3s, 3p, 3d, 4s, 4p, 4d, 5s, 5p, 4f, and 5d for U.

(28) (a) Pye, C. C.; Ziegler, T. *Theor. Chem. Acc.* **1999**, *101*, 396. (b) Klamt, A.; Schüürmann, G. *J. Chem. Soc., Perkin Trans.* **1993**, *2*, 799−805.

(29) (a) te Velde, G.; Bickelhaupt, F. M.; van Gisbergen, S. J. A.; Fonseca, Guerra, C.; Baerends, E. J.; Snijders, J. G.; Ziegler, T. *J. Comput. Chem.* **2001**, *22*, 931−967. (b) Fonseca, Guerra, C.; Snijders, J. G.; te Velde, G.; Baerends, E. J. *Theor. Chem. Acc.* **1998**, *99*, 391−403. (c) Baerends, E. J.; Autschbach, J.; Bérces, A.; Bo, C.; Boerrigter, P. M.; Cavallo, L.; Chong, D. P.; Deng, L.; Dickson, R. M.; Ellis, D. E.; Fan, L.; Fischer, T. H.; Fonseca Guerra, C.; van Gisbergen, S. J. A.; Groeneveld, J. A.; Gritsenko, O. V.; Grüning, M.; Harris, F. E.; van den Hoek, P.; Jacobsen, H.; van Kessel, G.; Kootstra, F.; van Lenthe, E.; McCormack, D. A.; Osinga, V. P.; Patchkovskii, S.; Philipsen, P. H. T; Post, D.; Pye, C. C.; Ravenek, W.; Ros, P.; Schipper, P. R. T.; Schreckenbach, G.; Snijders, J. G.; Sola, M.; Swart, M.; Swerhone, D.; te Velde, G.; Vernooijs, P.; Versluis, L.; Visser, O.; van Wezenbeek, E.; Wiesenekker, G.; Wolff, S. K.; Woo, T. K.; Ziegler, T. *ADF2004.01*; SCM, Theoretical Chemistry, Vrije Universiteit: Amsterdam, The Netherlands, 2004.

(30) Car, R.; Parrinello, M. *Phys. Rev. Lett*. **1985**, *55*, 2471−2474.

(31) *CPMD*, version 3.7.0; IBM Corp.: Armonk, NY, 1990−2001. MPI für Festkörperforschung: Stuttgart, Germany, 1997−2001.

(32) Troullier, N.; Martins, J. L. *Phys. Rev. B* **1991**, *43*, 1993−2006.

(33) Kleinman, L.; Bylander, D. M. *Phys. Rev. Lett*. **1982**, *48*, 1425−1428.

(34) It is difficult to ensure full equilibration after such a short time. In some cases, in particular for **4**, the simulations may just be metastable, and much longer simulation times might be needed to reach the true ground states. However, all observable parameters discussed, i.e. bond distances or mean constraint forces, were reasonably well converged within the duration of the simulations, without showing noticeable drifts.

(35) E.g.: Lax, E., Ed. *D'Ans-Lax Taschenbuch für Chemiker und Physiker*, 3rd ed.; Springer-Verlag: Berlin, 1967; Vol. 1.

Chart 1

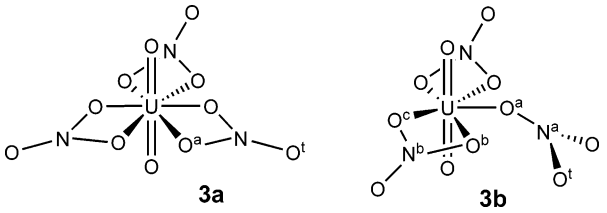

3a **3b**

interactions were treated with the Ewald method. No electrostatic decoupling between replicated cells was included, as it had been shown that no noticeable errors are introduced by this procedure even for divalent ions.[36] The CPMD(aq) simulations were started from well-equilibrated classical MD runs using the AMBER force field.[37]

Constrained CPMD and CPMD(aq) simulations were performed along predefined reaction coordinates connecting complexes with the indicated hapticities or coordination numbers, to evaluate the change in the Helmholtz free energy by pointwise thermodynamic integration (PTI)[38] of the mean constraint force $\langle f \rangle$ along suitable predefined reaction coordinates ξ via

$$\Delta A_{a\rightarrow b} = -\int_a^b \langle f(\xi) \rangle \, \mathrm{d}\xi \qquad (1)$$

For the η^2-to-η^1 transition of nitrate, the difference Δr between two U−O(nitrate) distances was chosen as reaction coordinate and was increased successively from zero in steps of 0.2 Å. At each point, the system was propagated until $\langle f \rangle$ was sufficiently converged (usually within 1.5−2 ps after 0.5 ps of equilibration, similar to the degree of convergence documented in Figure S1 of the Supporting Information for ref 20a).

Results and Discussion

This part is organized as follows: In the first section trinitrate **3** is studied (along with tetranitrate **4**) using structural information from experiment as starting point for the simulations. The second section is devoted to the mononitrate **1**, where no such information is available.

1. $[UO_2(NO_3)_3]^-$. The structure of this ion has been repeatedly characterized by neutron diffraction or X-ray crystallography[14] and, facilitated by its high symmetry, by quantum-chemical calculations.[39] An archetypical example of 6-fold coordination about uranyl, no evidence for reduction in hapticity of the bidentate nitrate ligands has been found. The optimized and simulated bond distances of the lowest minimum **3a** (Chart 1) are in good mutual accord between the various theoretical methods and agree reasonably well[40] with the experimental values in the solid state (Table 1).

What is interesting in the case of **3a** is the lack of any notable solvent effect on the geometrical parameters (compare ZORA and ZORA(aq) or CPMD and CPMD(aq) data in Table 1). For the neutral dinitrate dihydrate **2**, in contrast, much larger such effects had been noted:[20b] on going from CPMD to CPMD(aq), the U−O distance to the nitrate ligand increased from 2.51(8) to 2.59(24) Å (with concomitant decrease of the U−O bond length to the coordinated water molecules). For anionic **3a**, the uranyl−nitrate distance stays essentially the same upon hydration; there is a slight increase in mobility in water, however, as revealed by the slightly larger standard deviation of the U−ONO_2 distance, 0.06 Å vs 0.09 Å for CPMD vs CPMD(aq), respectively (Table 1). Despite the closer mutual contact of the negatively charged nitrate ligands in **3a**, as compared to those in **2**, the observed U−O(N) distances in the former are slightly shorter, by ca. 0.06 Å, than those in the latter.[41] The same trend, both qualitatively and quantitatively, is found in the CPMD(aq) data. In contrast, a much smaller discrimination between both forms is computed in the gas phase, where the U−O(N) distances in **3a** are consistently found to be ca. 0.02 Å longer than in **2**. The structural variations between uranyl dinitrates and trinitrates observed in the solid may thus not be intrinsic to these systems but may rather stem from differential effects of the polar environment.

We now turn to the question of nitrate hapticity, recalling the results obtained[20b] for the dinitrate **2** in the gas phase: Upon transformation of one nitrate ligand from the η^2 to a η^1 coordination mode, the resulting $UO_2(\eta^2\text{-}NO_3)(\eta^1\text{-}NO_3)\text{-}(H_2O)_2$ isomer was stabilized by an intramolecular hydrogen bond between one of the dangling O atoms of the monodentate nitrate and the adjacent water ligand, resulting in a rather unsymmetrical structure. No such interaction is possible in **3**, and the monodentate form $[UO_2(\eta^2\text{-}NO_3)_2(\eta^1\text{-}NO_3)]^-$ (**3b**) is essentially C_s-symmetric. Whereas the U atom forms a plane with the bidentate nitrates, the monodentate ligand is significantly bent out of this plane (see CP-opt value of the U−O−N angle, which is collected, together with other selected parameters, in Table 2). Similar orientations and

(36) Marx, D.; Hutter, J.; Parrinello, M. *Chem. Phys. Lett.* **1995**, *241*, 457−462.

(37) Case, D. A.; Pearlman, D. A.; Caldwell, J. W.; Cheatham, T. E., III; Wang, J.; Ross, W. S.; Simmerling, C. L.; Darden, T. A.; Merz, K. M.; Stanton, R. V.; Cheng, A. L.; Vincent, J. J.; Crowley, M.; Tsui, V.; Gohlke, H.; Radmer, R. J.; Duan, Y.; J. Pitera; Massova, I.; Seibel, G. L.; Singh, U. C.; Weiner, P. K.; Kollman, P. A. *AMBER7*; University of California: San Francisco, CA, 2002. The force field parameters used for the molecular dynamics simulations are from ref 21a.

(38) Sprik, M.; Ciccotti, G. *J. Chem. Phys.* **1998**, *109*, 7737−7744 and references cited therein.

(39) See e.g.: (a) Pyykkö, P.; Li, J.; Runeberg, N. *J. Phys. Chem.* **1994**, *98*, 4809−4813. (b) de Jong, W. A.; Aprà, E.; Windus, T. L.; Nichols, J. A.; Harrison, J. H.; Gutowski, K. E.; Dixon, D. A. *J. Phys. Chem. A* **2005**, *109*, 11568−11577.

(40) That is, metal−ligand bond distances are overestimated by several picometers (up to ca. 7 pm), which is not uncommon for this particular functional (see, e.g.: Bühl, M.; Kabrede, H. *J. Chem. Theory Comput.* **2006**, *2*, 1282−1290). This is true both for equatorial U−O and axial U═O distances. A reviewer has voiced concerns concerning the credibility of the computed energies if the geometry of the central uranyl unit is associated with such an error. Because the errors in the geometrical parameters are fairly systematic throughout (see Tables 1 and 3 in this paper and Table 3 in ref 20b), the *relative* energies should be affected only to a small extent. Even the error in terms of *absolute* energies is indicated to be quite small: According to single-point energy computations at a sophisticated multireference ab initio level for a uranyl hydrate complex, a BLYP/SCRF-optimized geometry (despite its elongated U═O distances) is only 0.9 kcal/mol higher in energy than the corresponding B3LYP/SCRF geometry (which shows more accurate U═O bond lengths); see Table 5 in ref 51b. Unfortunately, the use of hybrid functionals such as B3LYP is prohibitively expensive with CPMD.

(41) Mean r(U−ONO_2) values in the solid: 2.53 Å. See e.g.: (a) Charushnikova, I. A.; Den Auwer, C. *Koord. Khim.* **2004**, *30*, 546−554; *Russ. J. Coord. Chem.* **2004**, *30*, 511−519 (ref-code AZECUD). (b) Villiers, C.; Thuery, P.; Ephritikhine, M. *Polyhedron* **2004**, *23*, 1613−1618 (ref-codes AZOTAK and AZOTEO).

Table 1. Geometrical Parameters (Bond Distances in Å)[a] of **3a**, Computed with the BLYP Functional and Observed in the Solid

param	LANL	ZORA	CP-opt	CPMD	ZORA(aq)	CPMD(aq)	X-ray[b]
r(U═O)	1.83	1.82	1.81	1.82(2)	1.82	1.81(4)	1.75
r(U−O^a)	2.56	2.53	2.51	2.53(6)	2.52	2.53(9)	2.47
r(N−O^t)	1.24	1.23	1.23	1.23(2)	1.23	1.22(2)	1.21
r(N−O^a)	1.30	1.31	1.31	1.31(2)	1.31	1.31(2)	1.28

[a] Averaged values, where appropriate. In parentheses, standard deviations over the CPMD trajectories (last 1.5 ps). [b] From ref 14 (standard deviations quoted between 0.004 and 0.009 Å; counterion NO^+).

Table 2. Selected Geometrical Parameters (Bond Distances in Å, Angles in deg)[a] and Relative Energies (kcal/mol) Computed for **3b** in the Gas Phase (CP-opt and CPMD) and in Aqueous Solution (CPMD(aq))

param	CP-opt	CPMD	CPMD(aq)[b]
r(U═O)	1.81	1.82(4)	1.81(3)
r(U−O^a)	2.30	2.29(4)	2.29(3)
r(U−O^b)	2.48	2.51(6)	2.49(7)
r(U−O^c)	2.51	2.49(9)	2.52(7)
r(U···O^t)	4.00	4.07(21)	4.03(7)
a(U−O^a−N^a)	132.5	135(7)	132(4)
rel energy	4.0[c]	6.3[d]	na

[a] Averaged values, where appropriate. In parentheses, standard deviations over the CPMD trajectories (last 1.5 ps). See Chart 1 for labeling of atoms. [b] From a constrained MD simulation (averaged over 0.5−1.1 ps); see text. [c] Optimized potential energy ΔE relative to **3a**. [d] Free energy ΔA relative to **3a**.

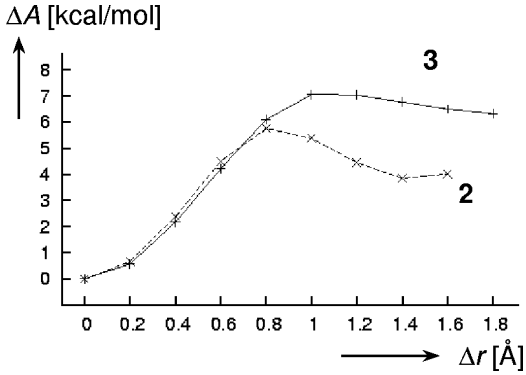

Figure 1. Change in free energy, ΔA, for η^2-to-η^1 transition of one nitrate ligand in $[UO_2(NO_3)_3]^-$ (**3**, solid line), as obtained from constrained CPMD simulations and thermodynamic integration in the gas phase (reaction coordinate: difference Δr between two U−O(nitrate) distances). Dashed line: corresponding ΔA profile for $UO_2(NO_3)_2(OH_2)_2$ (**2**) from ref 20b.

values for U−O−N angles have been observed in solid η^1-nitrate uranyl complexes (with angles between 125 [17b] and 139° [17a]).

We have subsequently performed constrained MD simulations along a path connecting **3a** and **3b** for evaluation of their relative free energies via thermodynamic integration (see Computational Details and previous applications of this technique to uranyl complexes[20]). Using the difference of the U−O distances to two O atoms of the same nitrate as reaction coordinate (i.e., $\Delta r = r(U{-}O^t) - r(U{-}O^a)$ for **3b** in Chart 1), we obtained the free-energy profile depicted in Figure 1 (solid curve). Starting from the minimum **3a** at $\Delta r = 0$, the η^1-form **3b** is reached at $\Delta r \approx 1.8$ Å, at which point the mean constraint force is essentially zero. This point is higher in free energy than the starting point by $\Delta A = 6.3$ kcal/mol, with a barrier of $\Delta A^{\ddagger} = 7.1$ kcal/mol at $\Delta r \approx 1.0$ Å.

The corresponding ΔA profile of the dinitrate **2** from ref 20b is included in Figure 1 (dashed line). It is noteworthy that up to $\Delta r = 0.8$ Å both curves are essentially coinciding. After that point the stabilizing H-bonding interaction sets in for **2**, causing ΔA to drop significantly, whereas, for **3**, ΔA continues to rise until $\Delta r = 1.0$ Å and ends up in the shallow η^1-minimum **3b** at $\Delta r \approx 1.8$ Å. The relative energy of **3b** with respect to **3a** is somewhat lower on the potential energy surface (4.0 kcal/mol; see CP-opt value in Table 2) than on the ΔA profile (6.3 kcal/mol). For the dinitrate **2**, the opposite had been found, with ΔE and ΔA values for the η^2-to-η^1 transition of 6.2 and 3.9 kcal/mol, respectively.[20b] The reason for this qualitative difference is not fully clear, but it appears that when dynamical effects are taken into account, this transition is less favorable for **3** than for **2**.

When an unconstrained MD is started from the equilibrium geometry of the η^1-form **3b** in the gas phase, the molecule stays in this conformation for at least 1.5 ps. It is from this trajectory (excluding the first 0.5 ps), where the averaged geometrical parameters in Table 2 are taken from. The mean unconstrained value for $\Delta r = r(U{\cdots}O^t) - r(U{\cdots}O^a) = 1.78$ Å corresponds very well to that of the final point of the constrained path (1.8 Å; see Figure 1). Interestingly, when the simulation of that final point was continued without the constraint, the η^1-bonded nitrate immediately (within ca. 0.4 ps) reverted to the more favorable bidentate coordination mode. The rapid and irreversible occurrence of the η^1-to-η^2 rearrangement is fully consistent with the substantial thermodynamic driving force for this process, as discussed above.

Closer inspection of the trajectory with the rapid rearrangement revealed that the starting point, that is, the last point from the constrained MD run, featured one rather large $O^b{-}U{-}O^a$ angle exceeding 110°. This instantaneous structure thus is significantly distorted toward a complex with a vacant coordination site, into which, apparently, the subsequent rotation of the nitrate ligand with one of its dangling O atoms is readily possible. The evolution of the angle in question during the constraint and after its release is monitored in Figure 2. Note how this angle undergoes large-amplitude oscillations around a mean value of ca. 90° during the first 2 ps, where the η^1-mode (i.e., **3b**) is preserved by the constraint, that it has fortuitously reached its maximum value right when the constraint is released, and how it rapidly closes to an average around 70° after that release of the constraint and formation of the η^2-minimum **3a**. These data serve to rationalize the different outcome of the two simulations with different starting conditions, which started either from a minimum or from an activated structure predisposed for the process under scrutiny.

It would be highly desirable to study the η^2-to-η^1 transition in an aqueous solution of **3a** with the same thermodynamic

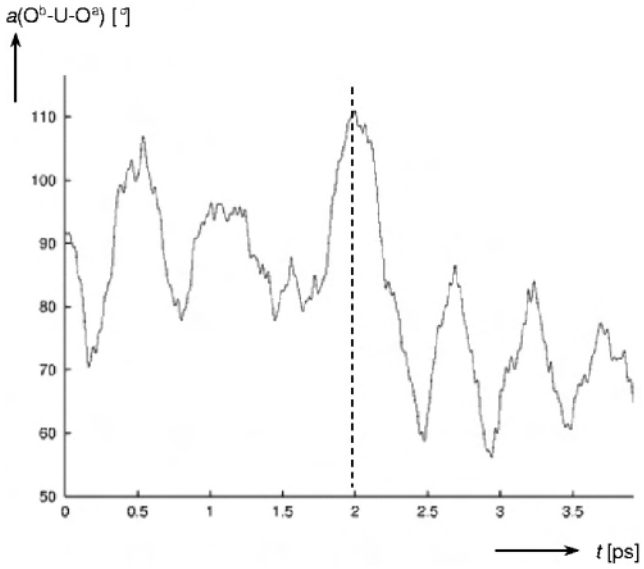

Figure 2. Evolution of the O^b-U-O^a angle (see Chart 1 for definition) in a CPMD simulation of **3b** in the gas phase: 0−2 ps, Δr constrained to 1.8 Å; after 2 ps (denoted by the dashed line), release of this constraint.

integration scheme used to generate the gas-phase profile in Figure 1. Unfortunately, due to the larger size of the box compared to that used for **2** (or **4**; see below), the long total simulation time required for this procedure (up to ca. 20 ps in total) would render this approach extremely expensive. Therefore, we just attempted to perform an unconstrained simulation for monodentate **3b** in water, to see if any spontaneous rearrangement to **3a** would be observed. To avoid artifacts from the instantaneous starting configuration, we first equilibrated aqueous **3b** for 0.5 ps by maintaining the η^1 binding mode of one nitrate via the usual distance constraint (Δr fixed to the gas-phase equilibrium value of 1.7 Å; cf. CP-opt data in Table 2). When this constraint was lifted, the monodentate nitrate ligand immediately rearranged to bind in bidentate fashion,[42] a process which was completed after ca. 0.5 ps (see plot of the salient distances in Figure 3). Thus, as in the gas phase, the η^2 binding mode about uranyl is also preferred in water.[43]

To obtain some structural data for the elusive monodentate form **3b** in water, we continued the constrained simulation for another 0.6 ps (i.e., past the point designated by the dashed line in Figure 3), which was then used to extract the CPMD(aq) parameters collected in Table 2. As with the η^2-congener **3a**, the solvation effect on the geometry is remarkably small.

(42) At the point of constraint release, the largest O^b-U-O^a angle had attained an instantaneous value of 87°; i.e. there was no apparent predisposition for a vacant coordination site, as discussed above for the corresponding event in the gas phase.

(43) Apparently, the monodentate form is not even metastable but unstable in water. In contrast, the corresponding η^1-variant of the dinitrate **2**, as it had emerged at the end of a constrained MD path, had remained metastable for 1 ps after lifting the constraint.[20b] It is thus tempting to speculate that the driving force for the η^1-to-η^2 transition in water should be larger for **3** than for **2**, as it is found in the gas phase (cf. Figure 1). For the dinitrate **2**, solvation was indicated to stabilize the monodentate binding mode by 2.5 kcal/mol with respect to the situation in the gas phase, presumably due to a better solvation of terminal vs uranyl-coordinated nitrate O atoms.[20b] Assuming a similar effect in the case of **3b** vs **3a**, a free energy difference on the order of 6.3 − 2.5 ≈ 4 kcal/mol could be expected between both in water.

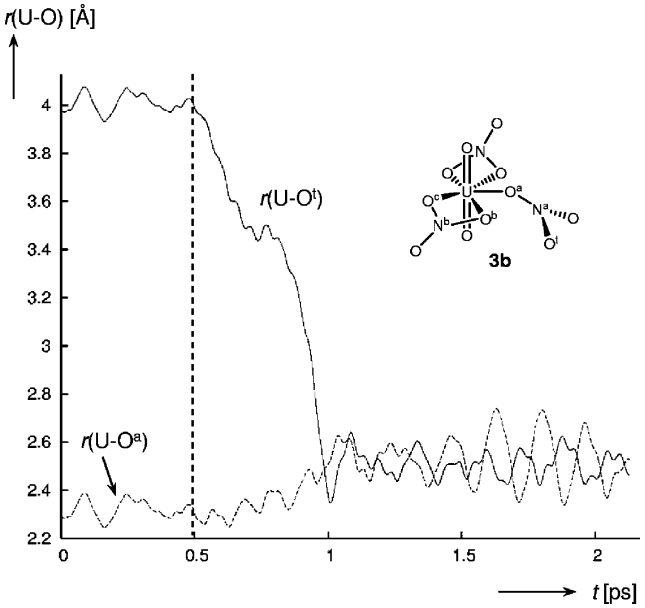

Figure 3. Evolution of U−O(nitrate) bond distance in a CPMD simulation starting from **3b** in water; 0−0.5 ps: constrained MD enforcing a constant difference Δr between both designated bonds; vertical dashed line: release of constraint.

A well-known species containing both mono- and bidentate nitrate ligands is **4**, which should be formulated as $[UO_2(\eta^2\text{-}NO_3)_2(\eta^1\text{-}NO_3)_2]^{2-}$. Geometrical parameters optimized or simulated in the gas phase and in water are summarized in Table 3. In this case, solvation is indicated to leave the distance to the monodentate nitrate ligand unaffected,[44] whereas those involving the bidentate ligands, $r(U-O^b)$ and $r(U-O^c)$, decrease noticeably upon solvation (compare CPMD and CPMD(aq) values in Table 3).

2. $[UO_2(NO_3)(H_2O)_4]^+$. We now turn to the mononitrate **1**. Even though, to our knowledge, this species has not been structurally characterized so far,[45] its existence in solution is quite plausible (e.g., at elevated nitrate concentration) and has in fact been inferred from electronic spectra.[11] Actually, given the low complexation constants between uranyl and nitrate, which are indicated to decrease with an increasing number of nitrate ions,[9] the mononitrate may well be the most abundant species in the aqueous phase. Nothing is known about the number of coordinated water molecules or the CN about uranyl in this species. With monodentate ligands coordinating through first-row atoms, five-coordination about uranyl is quite common.[16] On the other hand, six-coordination is frequently observed with chelating ligands with a small bite angle, such as nitrate. In fact, six-coordination is the rule when at least two nitrate ligands are present.[13−15] It appeared difficult to predict a CN for the mononitrate, and we decided to start our investigation with the highest possible CN, 6, as in the complex $[UO_2(\eta^2\text{-}NO_3)(H_2O)_4]^+$ (**1a**).

(44) It should be emphasized again at this point that there is no experimental evidence for the existence of **4** in aqueous solution. Arguably one or more nitrate ligands would eventually dissociate from **4** in water, even at high nitrate concentration. This process, apparently, happens on a somewhat longer time scale than that of our simulation.

(45) Uranyl mononitrate complexes are much less common than dinitrate species and are occasionally found in conjunction with other chelating ligands; see e.g. refs 17a,d,e.

Table 3. Geometrical Parameters (Bond Distances in Å, Angles in deg)[a] of **4**, Computed with the BLYP Functional and Observed in the Solid

param	LANL	CP-opt	CPMD	CPMD(aq)	X-ray[b]
r(U=O)	1.83	1.81	1.81(2)	1.82(2)	1.75
r(U−O^a)	2.52	2.44	2.45(9)	2.45(10)	2.43
r(U−O^b)	2.65	2.60	2.64(13)	2.59(10)	2.51
r(U−O^c)	2.65	2.62	2.64(11)	2.57(9)	2.51
a(U−O^a−N^a)	127.5	134.3	136(9)	128(6)	125.0

[a] Averaged values, where appropriate. In parentheses, standard deviations over the CPMD trajectories (last 1.5 and 1.1 ps in gas phase and in water, respectively). [b] C_i symmetry, from ref 15 (counterion dimethylimidazolium).

Chart 2

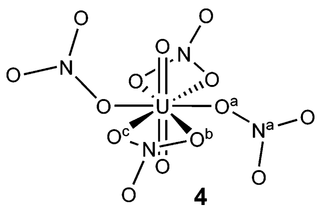

4

When an unconstrained CPMD simulation was started for **1a** in water, this species was only stable for ca. 0.5 ps, at which point the nitrate ligand spontaneously reverted to a monodentate coordination, affording $[UO_2(\eta^1\text{-}NO_3)(H_2O)_4]^+$ (**1b**; see Chart 3). This species underwent no further transformations for the remainder of the simulation, 4 ps in total. In the gas phase, minima corresponding to both **1a**,**b** can be located, but when CPMD simulations were started from either of these, one of the coordinated water molecules immediately (within 0.5 ps) detached, accepting a hydrogen bond from one of the other water ligands. A representative isomer of the resulting microsolvated complex $[UO_2(\eta^2\text{-}NO_3)(H_2O)_3]^+{\cdot}H_2O$ (**1c**) was subsequently optimized in the gas phase from the last point of one of these CPMD simulations. Salient geometrical and energetic data are summarized in Table 4.

In the gas phase, the microsolvated species **1c** is the most stable one, ca. 8−10 kcal/mol below **1a**,**b**, which are computed quite close in energy (see CP-opt energies in Table 4). To assess the relative stabilities in water, Helmholtz free energies were obtained by pointwise thermodynamic integration (PTI)[38] according to eq 1.

First, a pathway was constructed connecting **1a** and **1b** with $\xi = \Delta r = [r(\text{U−O}^b) - r(\text{U−O}^a)]$ as reaction coordinate. To this end, we took that part from the unconstrained simulation of **1a**, which marked the spontaneous **1a** → **1b** rearrangement discussed above, and selected snapshots from the trajectory where Δr was close or equal to 0, 0.2, 0.4, ..., or 1.4 Å. These snapshots were taken as starting points for constrained MD simulations with Δr frozen at the corresponding value. In all these runs, no further rearrangements were encountered, except for $\Delta r = 0$ (marking **1a**), where one of the four water ligands was expelled into the solution after ca. 0.6 ps. The mean constraint force was quite small near before this event, ca. 0.001 au, but this is, of course, not a properly equilibrated value. It turned out that the equilibrated values of $\langle f \rangle$ for Δr between 0.2 Å and 1.0 Å are small and positive, continually rising in magnitude to values around ca. 0.004 a.u. According to eq 1, this implies a drop in free energy with increasing Δr. By symmetry, the same drop in free energy is to be expected when going to the respective negative values of Δr. Symmetrical **1a** in aqueous solution therefore appeared to be a transition state rather than a minimum, and $\langle f \rangle$ was assumed to be zero for $\Delta r = 0$. With this procedure, the free energy profile shown in Figure 4a was obtained.[46]

The lowest point on this profile is found at $\Delta r = 1.2$ Å (corresponding to **1b**), 2.8(±0.6) kcal/mol lower in free energy than **1a**. As in our previous PTI studies,[20] the uncertainty was estimated from the largest standard deviation of the running average of $\langle f \rangle$ during the last 1 ps of the constrained run, multiplied with the total integration width.[47] There is a small but pronounced driving force for reducing the hapticity of the nitrate ligand in **1a**, consistent with the spontaneous formation of **1b** during the unconstrained CPMD simulation in water.

To assess the stability of **1c**, we constructed a second PTI pathway, namely for water dissociation from **1a**. In this case (analogous to uranyl pentahydrate),[20a] we used a simple U−O distance as constraint, specifically $\xi = r(\text{U−O}^d)$, i.e. the distance to that water ligand (trans to the nitrate; see Chart 3) that detached spontaneously in the above-mentioned constrained MD with $\Delta r = 0$. Prior to that dissociation, r(U−O^d) oscillated around 2.62 Å,[48] which was taken as starting point for integration with assumed $\langle f(r) \rangle = 0$ (no constrained MD was performed for that point, because it is to be expected that this structure will not remain stable with this single constraint, as it can reduce its coordination number by other processes, e.g., by reverting to **1b**). Again, the path was constructed by selecting snapshots from a trajectory describing the desired rearrangement, this time from the above-mentioned water dissociation from **1a** with values for r(U−O^d) close or equal to 2.8, 3.0, ..., or 4.4 Å[49] and by performing constrained MD simulations for each of these with r frozen at the corresponding value. In essentially all cases, near-

(46) Because on going from $\Delta r = 1.0$ to 1.2 Å the mean constraint force showed a large drop from $\langle f \rangle = 0.0042$ to -0.0010 au, an additional point for $\Delta r = 1.1$ Å was computed.

(47) This uncertainty refers to the numerical precision of the PTI technique. The absolute uncertainty due to the accuracy of the underlying quantum-chemical methodology (density functional, pseudopotential, basis set) is, arguably, considerably higher and is at least ±2.5 kcal/mol, judged from the errors in computed kinetic and thermodynamic parameters relative to experiment.[20c,d] However, computed relative trends between related systems, such as the driving force for the bi- to monodentate transition in the various nitrate species, should be reliable.

(48) The slightly different value in Table 3, 2.59 Å, is the average with the formally equivalent U−O distance with a mean r(U−O) value of 2.57 Å. There was thus already a noticeable predisposition for dissociation of one particular water molecule that had developed during this short time.

(49) At $r(\text{U−O}^d) = 4.4$ Å, the end point of this predefined coordinate, the mean constraint force was not yet zero ($\langle f \rangle = 0.0019$ au); hence, another point with $r = 4.5$ Å was computed.

Table 4. Selected Geometrical Parameters (Bond Distances in Å)[a] and Relative Energies (kcal/mol) Computed for **1a**−**c** in the Gas Phase (CP-opt and CPMD) and in Aqueous Solution (CPMD(aq))

	1a		**1b**		**1c**		
param	CP-opt	CPMD(aq)	CP-opt	CPMD(aq)	CP-opt	CPMD	CPMD(aq)
r(U−O^a)	2.46	2.61(9)	2.30	2.46(9)	2.44	2.45(8)	2.54(10)
r(U−O^b)	2.46	2.61(9)	3.73	3.71(16)	2.44	2.45(8)	2.54(10)
r(U−O^c)	2.66	2.52(8)	2.46	2.47(10)	2.43	2.51(12)	2.43(7)
r(U−O$^{c'}$)	2.66	2.52(8)	2.56	2.47(10)	2.53	2.58(9)	2.43(7)
r(U−O^d)	2.63	2.59(12)	2.56	2.47(9)	2.52	2.61(10)	2.43(7)
r(U···N)	2.95	3.05(10)	3.39	3.28(19)	2.95	2.90(6)	2.98(8)
rel energy	−1.6[b]	2.8[c]	0.0	0.0	−8.7[b]	na[d]	2.5[c]

[a] Averaged values, where appropriate. In parentheses, standard deviations over the CPMD trajectories. Gas phase: last 1.5 ps. In water: **1a**, first 0.5 ps of constrained MD (see text); **1b**, last 3 ps; **1c**, 2 ps. See Chart 3 for labeling of atoms. [b] Optimized potential energy ΔE relative to **1b**. [c] Free energy ΔA relative to **1b**. [d] No relative free energy available in the gas phase, because it is difficult to devise suitable reaction coordinates; see text.

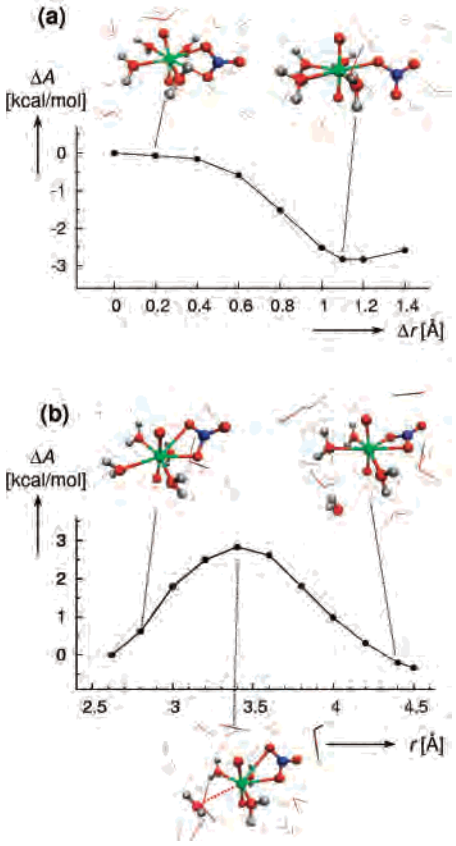

Figure 4. Change in free energy, ΔA, for rearrangements starting from aqueous **1a**, as obtained from constrained CPMD simulations and thermodynamic integration: (a) η^2-to-η^1 transition of the nitrate ligand affording **1b** (reaction coordinate: difference Δr between two U−O(nitrate) distances); (b) dissociation of one water ligand affording **1c** (reaction coordinate: U−O(water) distance r). Representative snapshots from indicated points are included.

perfect η^2-coordination of the nitrate was preserved, with very similar mean values for r(U−O^b) and r(U−O^a) (which were identical with each other in the starting frame but free to evolve from there on). The only exception was the point closest to **1a**, at r(U−O^d) = 2.8 Å, where the two mean U−O(nitrate) distances were found to differ by 0.09 Å. In judgment from the profile in Figure 4a, however, this small difference should have no significant consequences on the resulting energetics.

The resulting free-energy profile for this path is depicted in Figure 4b. Despite the fact that the initial starting geometries for each point were taken from a trajectory of a

Chart 3

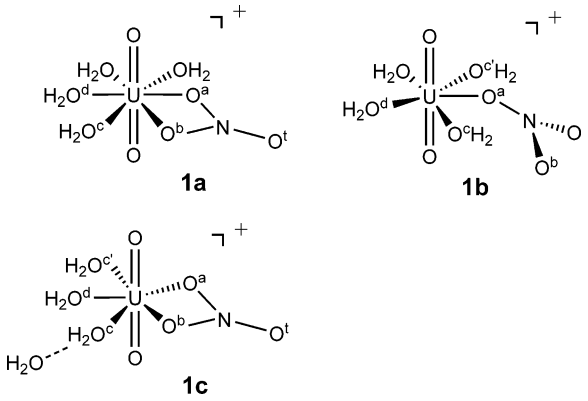

spontaneous process (with constrained bidentate nitrate; see above), a notable dissociation barrier is obtained in the PTI procedure, $\Delta A^{\ddagger}$ = 2.5 kcal/mol at r = 3.4 Å. For each of these starting structures between r = 2.8 Å and r = 3.4 Å, the initial instantaneous values for $f(r)$ were indeed positive, consistent with a driving force toward dissociation inherent in those particular frames. Proper equilibration, however, resulted in negative values for the ensemble-averaged $\langle f(r) \rangle$ values in each of these cases, affording the rise in free energy apparent in Figure 4b.[50] This finding emphasizes once more that one has to be cautious not to overinterpret singular spontaneous events in MD simulations.

At the end of this path, when the detached water molecule has been incorporated into the second hydration sphere, aqueous **1c** is computed to be only slightly more stable than **1a**, namely by ΔA = −0.3 kcal/mol. Using the same criteria as described above, the free energies evaluated from the path in Figure 4b are associated with an uncertainty of ca. ±1.0 kcal/mol,[47] i.e. somewhat larger compared to those from the path in Figure 4a, which is mainly rooted in the larger integration width. Prolonging all MD runs for improved statistics would arguably produce lower estimated errors. However, we are confident that this procedure, while being associated with considerable computational expense, would

(50) Provided that the phase space has been properly sampled in the constrained MD simulations, the free energies from PTI contain entropic contributions that are absent in the unconstrained MD runs, as the latter (in both Born−Oppenheimer and CPMD variants) are guided by the instantaneous gradients on the potential energy surface. If anything, the resulting $\Delta A^{\ddagger}$ and ΔA values for this dissociative process should thus be lower (more negative) than the corresponding potential energies, $\Delta E^{\ddagger}$ and ΔE.

Scheme 2

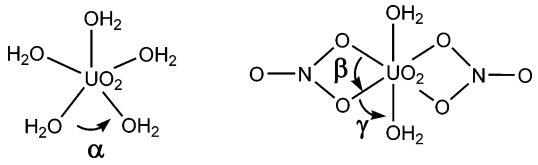

not change the qualitative finding, namely that **1a**,**c** are very close in their relative free energies in water.

The actual interconversion between **1b** and **1c** does not necessarily have to involve **1a**. At least in principle, the changes in free energies evaluated from eq 1 should be independent of the particular choice of ξ. Since **1a**,**c** are indicated to be of comparable stability in water and since aqueous **1b** is computed to be noticeably lower in free energy than **1a**, it thus follows that **1b** is also favored over **1c**, albeit only slightly. With the particular methodology that we have employed, the energetic discrimination between aqueous **1a**−**c** is not very pronounced, and a slight preference for **1b** with a monodentate nitrate is predicted. Six-coordinate **1a** with a bidentate nitrate ligand is clearly disfavored, as it does not appear to exist for more than ca. 1 ps in an unconstrained MD.

Why is six-coordination about uranyl possible in **2**−**4** but not in **1**? The small bite angle of a bidentate nitrate is likely to be an important factor. For a more quantitative interpretation, we evaluated mean values for the various types of O−U−O bond angles in the previous CPMD simulations of aqueous $[UO_2(H_2O)_5]^{2+}$ and **2** (α, β, and γ in Scheme 2). The resulting mean values for α, β, and γ are 72(5), 50(1), and 66(4)°, respectively (during the last 2 ps in each trajectory; standard deviation in parentheses). For **1a**, an angle sum of $3\alpha + \beta + 2\gamma = 398°$ would be predicted on these grounds, clearly too large to accommodate all six O atoms in the equatorial plane. In line with this simple reasoning, structures resembling **1a** develop a pronounced tendency for nonplanar orientation of these atoms in the course of the constrained MD simulations (note, e.g., that in the corresponding snapshots on the left-hand sides of Figure 4 the nitrate ligand is twisted out of the equatorial plane). A similar strongly nonplanar orientation is found in the solid state for a η^1-bonded uranyl nitrate with another pentadentate ligand[17e] (i.e., with six-coordination). In contrast, and in agreement with our findings for **1**, two bidentate or one tetradentate chelating ligands with larger bite angles favor five-coordination about uranyl and can accommodate an additional nitrate only in η^1-bonding mode.[17a,d]

There is evidence that common density functionals (including BLYP) tend to underestimate metal−ligand binding energies.[51] For instance, the free-energy difference between uranyl penta- and hexahydrate, decisive for the activation barrier for water exchange in the pentahydrate, is underestimated by ca. 2 kcal/mol with our CPMD/PTI methodology.[20c] The steric congestion just discussed for **1a**, however, should not be affected significantly by this argument.

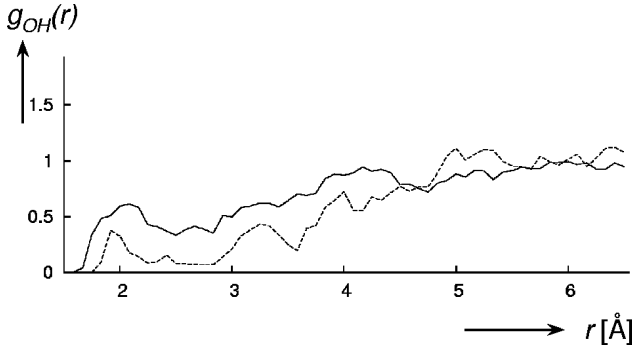

Figure 5. Partial radial distribution functions $g_{OH}(r)$ between the nitrate O atoms of **1b** and H atoms from the bulk: solid line, terminal nitrate O atoms; dashed, uranyl-coordinated nitrate O atom.

It would be desirable to compare the free-energy profiles in Figure 4 to corresponding ones obtained in vacuo to gauge the effect of the solvent. Because **1a**,**b** are intrinsically unstable in the gas phase, however, it will be very difficult to devise suitable reaction coordinates that would prevent the system from falling into the thermodynamic sink represented by **1c** (cf. the analoguous situation with uranyl hexahydrate[20c]). At the moment, the best we can compare our solution-phase ΔA values to are static gas-phase energies, e.g., the CP-opt energies ΔE (Table 4) or ΔG values derived thereof, by adding enthalpic and entropic corrections from harmonic frequency calculations. When the latter, obtained at the LANL level, are added to the CP-opt energies, the estimated relative free energies for **1a**−**c** are 0.8, 0.0, and −8.0 kcal/mol, respectively, qualitatively similar to the ΔE values in Table 4, except that the sequence of the close-lying complexes **1a**,**b** is reversed. The most striking feature of the relative stabilities upon going from the gas phase into solution is the significant stabilization of **1a**,**b** with respect to **1c**. For **1a**, this stabilization amounts to ca. 7−8 kcal/mol (depending whether optimized ΔE or estimated ΔG values are considered for the gas phase). A qualitatively similar, if somewhat smaller, stabilization (ca. 4 kcal/mol) had been obtained for uranyl hexa- vs pentahydrate,[52] and a slightly larger one had been found for uranyl penta- vs tetrahydrate (ca. 10 kcal/mol).[20a] In all these cases, solvation thus favors the complex with the higher coordination number.

The water-induced stabilization of **1b** with respect to **1c**, ca. 11 kcal/mol, is noteworthy, as both have the same coordination number. The former has a larger number of water molecules attached to uranium; however, the bonding to which is reinforced in solution (compare the corresponding CP-opt and CPMD(aq) entries for $r(U-O^c)$, $r(U-O^{c'})$, and $r(U-O^d)$ in Table 4). In addition, **1b** has a larger number of terminal nitrate O atoms, which can better interact with the solvent than directly coordinated ones.[20b] This differential solvation of the nitrate O atoms is illustrated in Figure 5, a plot of the respective partial radial distribution functions (RDFs) between these O atoms and H atoms from bulk water during 3 ps of simulation. Even though no strong peaks are found below $r = 2.5$ Å, there are shallow maxima in that

(51) See for instance for metal aqua ions: (a) Rotzinger, F. R. *J. Phys. Chem. B* **2005**, *109*, 1510−1527. (b) Rotzinger, F. R. *Chem.*−*Eur. J.* **2007**, *13*, 800−811.

(52) Obtained as difference between the relative energies of the hexahydrate, namely ΔE(gas) = 10.8 kcal/mol and ΔA(water) = 6.4 kcal/mol, as given in ref 20c.

area, around $r = 2$ Å, which originate from short-lived, specific O···H−O hydrogen bonds. These are visibly more frequent for the terminal O atoms (solid line) than for the coordinated atom (dashed line; note that the RDFs are normalized to the number of O atoms). When the RDFs in Figure 5 are integrated up to $r = 2.5$ Å, the resulting average numbers of H atoms within that distance are 1.2 and 0.4 around each terminal and coordinated nitrate O atom, respectively. Similar partial RDFs are obtained for **1c** (during 2 ps of unconstrained MD, not shown), confirming this preferred solvation of terminal vs coordinated O atoms.

EXAFS spectra of dilute (0.25 M) aqueous solutions of uranyl dinitrate **2** and of acidic uranyl hydrate with up to 1 M of nitrate present had been found to be essentially identical with those of the pristine hydrate (perchlorate counterion), which had been taken as evidence for complete dissociation of uranyl and nitrate ligands in water.[53] At this point it is interesting to note that the simulated equatorial ligand environment about uranyl is in fact virtually identical for aqueous $[UO_2(H_2O)_5]^{2+}$ and **1b**: according to our CPMD simulations, the former has five U−O contacts of 2.47(9) Å[20a] and the latter has also five such contacts between 2.46(9) and 2.47(10) Å (Table 4). Thus, even if the mononitrate would be populated to a significant extent in form of **1b**, it could not be distinguished from the pentahydrate by EXAFS if only the bonded region is considered (as had been done, e.g., in ref 53a). The presence or absence of mononitrate **1b** could probably be established if a significant contribution from an U−N absorber−backscatterer pair in the region around 3.3 Å could be detected or excluded (cf. r(U···N) value in Table 4). However, in view of the large vibrational amplitude of this distance (almost 0.2 Å standard deviation, Table 4) a critical evaluation of the sensitivity and the detection limit of this technique would be needed.[54]

A final point is worth elaborating, namely the barrier for water dissociation on the path depicted in Figure 4b. Relative to the most stable form **1b**, this barrier amounts to $\Delta A^{\ddagger} =$ 5.3 kcal/mol (the sum of the barrier relative to **1a**, 2.5 kcal/mol, and the energy of **1a** relative to **1b**, 2.8 kcal/mol). This value should be representative, even if only one of the four possible dissociation paths was followed and if the actual path for water dissociation from **1b** does not necessarily proceed via **1a**. For $[UO_2(H_2O)_5]^{2+}$, a much higher barrier has been computed for the corresponding process, namely $\Delta A^{\ddagger} = 10.8$ kcal/mol.[20a] Thus, the monodentate nitrate is not just an innocent spectator but can affect kinetic parameters significantly (see Figure 6).

The value of 5.3 kcal/mol is even lower than that computed for associative water exchange in the pentahydrate via a transient hexahydrate species, $\Delta A^{\ddagger} = 6.7$ kcal/mol at the same level[20c] (experiment: 9.1 kcal/mol),[55] which is the preferred route in the hydrate complex. Thus, replacement of one water moiety in $[UO_2(H_2O)_5]^{2+}$ with a nitrate ligand could not only accelerate the exchange between the remaining water ligands and the bulk solvent[56] but might even alter the whole subsitution mechanism, namely from I_a (or A) to D (or I_d). The latter possibility cannot be claimed with certainty, however, before an actual associative pathway is computed for **1b**. Interestingly, the preference for such a dissociative pathway for water exchange at a uranyl moiety has been predicted computationally for the $[UO_2F_4(H_2O)]^{2-}$ ion,[57] i.e. when four of the water ligands in $[UO_2(H_2O)_5]^{2+}$ have been replaced by negatively charged donors. It is to be expected that eventually, MD simulations as those presented here can help to understand and predict the way how rates and mechanisms of ligand substitution reactions at uranyl centers[58] can be tuned by the overall coordination environment about the metal.

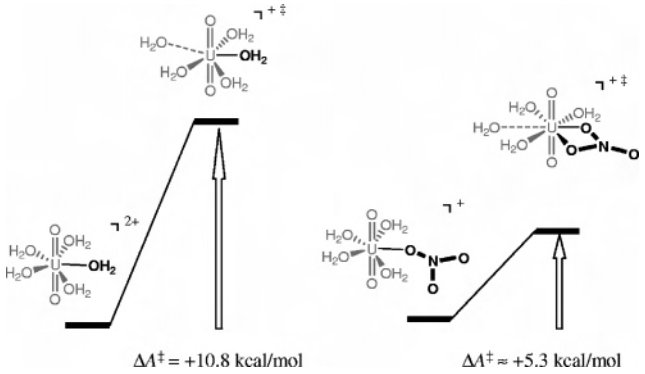

Figure 6. Schematic free energy barriers for water dissociation in $[UO_2(H_2O)_5]^{2+}$ (left) and **1b** (right), as obtained from CPMD simulations in water.

Conclusions

We have used CPMD simulations and thermodynamic integration to study structures of uranyl mono- and trinitrate complexes in vacuo and in water, calling special attention to the coordination mode of the nitrate ligand, monodentate vs bidentate. For the pristine trinitrate species **3**, η^1-coordination is computed to be higher in free energy by 6 kcal/mol than the common η^2-form, the latter of which is also preferred in aqueous solution. The six-coordinate, bidentate mononitrate with four additional water ligands (**1a**), in contrast, is indicated to be unstable: in the gas phase, it rapidly loses a water ligand to form a microsolvated five-coordinate complex (**1c**). In water, **1a**,**c** are essentially identical in their simulated free energies, and a second process becomes competitive, namely reduction of nitrate

(53) (a) Charpin, P.; Dejean, A.; Folcher, G.; Rigny, P.; Navaza, P. *J. Chim. Phys. Phys.-Chim. Biol.* **1985**, *82*, 925−932. (b) Shofield, P. F.; Bailey, E. H.; Mosselmans, J. F. W. In *Geochemistry of the Earths's Surface*; Armansson, Ed.; Proceedings of the 5th International Symposium on Geochemistry of the Earth's Surface; Balkema: Rotterdam, The Netherlands, 1999; pp 465−468. Review: (c) Antonio, M. R.; Soderholm, L. X-Ray Absorption Spectroscopy of Actinides. In *The Chemistry of the Actinide Elements*, 3rd ed.; Springer: Dordrecht, The Netherlands, 2006; pp 3087−3121.

(54) Interestingly, at very high temperatures (250 °C), evidence for nitrate coordination to uranyl has been found in an EXAFS analysis, with a coordination environment resembling that in **1c**.[53b]

(55) Farkas, I.; Bányai, I.; Szabó, Z.; Wahlgren, U.; Grenthe, I. *Inorg. Chem.* **2000**, *39*, 799−805.

(56) After dissociation of one water ligand from **1b** (affording the intermediate **1c**), another water molecule from the solvent can attach via the reverse pathway, thereby completing the water exchange process discussed.

(57) Vallet, V.; Wahlgren, U.; Szabó, Z.; Grenthe, I. *Inorg. Chem.* **2002**, *41*, 5626−5633.

(58) For a recent review, see: Szabó, Z.; Toraishi, T.; Vallet, V.; Grenthe, I. *Coord. Chem. Rev.* **2006**, *250*, 784−815.

hapticity, affording the five-coordinate η^1-mononitrate complex **1b**. It is this complex that is predicted to be favored over **1a** or **1c** in water, albeit only by less than 3 kcal/mol in terms of free energies. The simulated activation barrier for water dissociation from **1b** is only half of that in the parent pentahydrate, indicating that replacement of one water ligand in the latter by nitrate can affect the rate and possibly even the mechanism of water exchange at uranyl.

One factor contributing to the destabilization of hexacoordinate **1a** relative to the five-coordinate **1b** is indicated to be simply steric in nature, due to the larger "natural" bite angle of two adjacent water ligands, compared to that of a η^2-bonded nitrate. Hexacoordination in uranyl nitrate complexes is thus only expected with two or more nitrate ligands or other chelating groups.

Another factor contributing to the stability of **1b** in water is the better solvation of terminal vs coordinated O atoms of the nitrate ligands, as apparent in salient partial RDFs. Solvation thus favors η^1-coordination because of the concomitant increase in the number of terminal O atoms. This differential solvation may also be responsible for the absence of the "classical" chelate effect in the mononitrate. Despite the expected gain in entropy upon release of one water ligand during the transformation **1b** → **1c**, this process is predicted to be unfavorable in water. The structural question of η^1- vs η^2-bonded nitrate should have important consequences for extraction properties of uranyl complexes, as the former binding mode is expected to make the complexes more hydrophilic.

Acknowledgment. M.B. thanks W. Thiel, the MPI für Kohlenforschung, and the Deutsche Forschungsgemeinschaft for support. A generous allotment of CPU time on an IBM p690 "Regatta" cluster at Rechenzentrum Garching is gratefully acknowledged. R.D. and G.W. thank the CNRS-IDRIS, GDR Paris, and University Louis Pasteur for support. We appreciate additional support in the framework of a German−French exchange program (DAAD/PROCOPE).

Supporting Information Available: Optimized coordinates for **2**−**4**. This material is available free of charge via the Internet at http://pubs.acs.org.

IC0622555